Collective flow in p-Pb and d-Pb collisions at TeV energies

Piotr Bożek[1,2,*]

[1] *The H. Niewodniczański Institute of Nuclear Physics, PL-31342 Kraków, Poland*
[2] *Institute of Physics, Rzeszów University, PL-35959 Rzeszów, Poland*

(Dated: January 31, 2012)

We apply the hydrodynamic model to the dynamics of matter created in p-Pb collisions at $\sqrt{s_{NN}} = 4.4$TeV and d-Pb collisions at $\sqrt{s_{NN}} = 3.11$TeV. The fluctuating initial conditions are calculated in the Glauber Monte-Carlo model for several centrality classes. The expansion is performed event by event in $3+1$-dimensional viscous hydrodynamics. Noticeable elliptic and triangular flows appear in the distributions of produced particles.

PACS numbers: 25.40.Ep, 25.45.De, 13.85Hd, 25.75.Ld
Keywords: hadron-nucleus collisions, viscous hydrodynamic model, collective flow

I. INTRODUCTION

The large multiplicity of particles emitted from the small interaction region in relativistic heavy-ion collisions implies that a fireball of very dense matter is formed. Experiments at the BNL Relativistic Heavy Ion Collider (RHIC) and the CERN Large Hadron Collider (LHC) [1, 2] have demonstrated the appearance of a collective flow in the expanding fireball. The physical picture is expected to be different in the interaction of small systems, proton-proton, proton-nucleus or deuteron-nucleus. At RHIC energies the density of matter created in d-Au interactions is small and does not cause jet quenching [1]. d-Au and p-p interactions are treated as a baseline reference to evidence new effects in nucleus-nucleus collisions, beyond a simple superposition of nucleon-nucleon (NN) collisions. With the advent of proton-proton collisions at several TeV center of mass (c.m.) energies at the LHC, it has been suggested that some degree of collective expansion appears in high multiplicity p-p events [3–6]. However, no direct experimental evidence exist for such a collective expansion in p-p interactions.

At the LHC, p-Pb collisions can be studied in the future, experiments with d-Pb or other asymmetric systems are also possible, but with additional technical difficulties [7]. Estimates of the hadron production in p-Pb interactions at TeV energies take into account nuclear effects on the parton distribution functions, saturation effects, but do not assume the formation of a hot medium [7, 8]. Experiments with p-Pb beams should provide an input for models used in heavy-ion collisions for the calculation of dense medium effects on hard-probes.

The expected multiplicity and size of the interaction region in central p-Pb and d-Pb collisions at TeV energies are similar as in peripheral ($60-80\%$ centrality) Pb-Pb collisions at $\sqrt{s_{NN}} = 2.76$TeV [9]. This raises the possibility that hot and dense matter is formed in such collisions. For strongly interacting matter, the assumption of local equilibrium is a good approximation and relativistic hydrodynamics can be used to follow the evolution of the system [10]. Quantitative predictions for the elliptic flow have to account for finite deviations from local equilibrium in the rapidly expanding fluid [11–13].

In order to test the assumption of the formation of a dense fluid in p-Pb and d-Pb interactions and to estimate possible effects of its collective expansion, we apply the viscous hydrodynamic model to calculate the spectra of emitted particles. The goal of this study is to have a quantitative prediction of the elliptic and triangular flows and of the transverse momentum spectra for comparison with future experiments. The dynamically evolved density of the fireball from hydrodynamic simulations can be used in the calculations of the parton energy loss in such small systems.

The task requires the use of the most sophisticated version of the hydrodynamical model: event by event $3+1$-dimensional ($3+1$-D) viscous hydrodynamics. While a good description of many collective phenomena in heavy-ion collisions can be obtained in the perfect fluid hydrodynamics in $2+1$-D [10, 14] or $3+1$-D [15], to calculate the azimuthally asymmetric flow in small systems such as p-Pb or d-Pb collisions one has to use viscous hydrodynamics. In collisions of symmetric nuclei $2+1$-D boost-invariant viscous hydrodynamics is routinely being applied for observables at central rapidities [11, 12]. In p-Pb or d-Pb interactions the energy density and the final particle distributions depend strongly on rapidity. This forces the use of $3+1$-D hydrodynamics to obtain realistic particles spectra at different rapidities. Only recently $3+1$-D viscous hydrodynamic simulations became available [13, 16]. In proton or deuteron interaction with a nucleus the shape of the interaction region fluctuates widely from event to event. Unlike in interactions of heavy ions, using the average density is not a reliable approximation. Event by event $3+1$-D perfect fluid hydrodynamics is used by several groups [17]. The inclusion of event by event fluctuations is important in the description of the initial eccentricity and triangularly of the fireball [13, 17–21]. Only one group is using an event by event $3+1$-D viscous hydrodynamic code for heavy-ion collisions [13, 22].

As the size and the life-time of the system decrease the

* Piotr.Bozek@ifj.edu.pl

hydrodynamic model becomes less justified. A sizable elliptic flow is observed in peripheral Pb-Pb collisions at the LHC, which proves that substantial rescattering occurs in the evolution of the fireball. By itself it does not prove that the hydrodynamic regime is applicable in such collisions, as some elliptic flow can be generated through collisions in the dilute limit. Few hydrodynamic calculations are applied also to peripheral Pb-Pb collisions at $\sqrt{s} = 2.76$TeV [3, 23, 24] with results compatible with experimental observations. Nevertheless, it must be noted that as the impact parameter increases, uncertainties of the hydrodynamic model become more important; fluctuations modify substantially the initial eccentricity, the relative role of the hadronic corona in the evolution of the system increases. In the present calculation the last issue is partly taken into account through an increase of the shear viscosity to entropy ratio at lower temperatures. For d-Au collisions at $\sqrt{s_{NN}} = 200$GeV the hydrodynamic model is expected to break down, as indicated by the absence of jet quenching. However, there are no published experimental results concerning directly the elliptic flow in d-Au collisions or estimates from hydrodynamic models at RHIC energies.

Below we present results from event by event viscous hydrodynamic simulations for p-Pb and d-Pb collisions at $\sqrt{s_{NN}} = 4.4$ and 3.11TeV respectively. We use Glauber Monte-Carlo model initial conditions for the hydrodynamic evolution. We calculate particle spectra, charged particle pseudorapidity distributions, elliptic and triangular flow coefficients as function of pseudorapidity and transverse momentum.

system	$\sqrt{s_{NN}}$ TeV	σ_{NN} mb	$\frac{dN}{d\eta_{PS}}$ at $\eta_{ps} = 0$
p-Pb	4.4	66.4	50 ± 5
	8.8	73.4	65 ± 9
d-Pb	3.11	63	80 ± 5
	6.22	69.8	95 ± 10

TABLE I. NN cross section (third column) and expected density of charged particles at mid-rapidity in the NN c.m. (fourth column) for different systems and energies in central collisions.

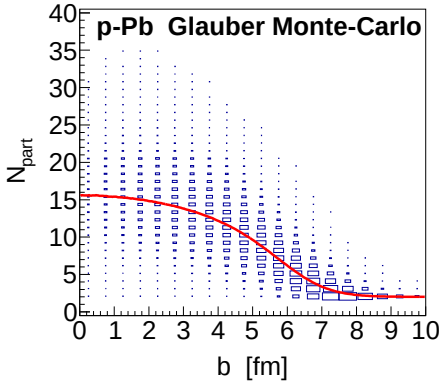

FIG. 1. (Color online) The distribution of participant nucleons at different impact parameters (boxes) and the average number of nucleons as function of the impact parameter (solid line) for p-Pb interactions.

II. SIZE AND SHAPE OF THE INITIAL FIREBALL

The number of particles produced in a p-Pb or d-Pb interaction can be estimated from N_{part} the number of participant (wounded) nucleons in collision. The Glauber Monte-Carlo model generates a distribution of events with different source sizes (number of participant nucleons) and different shapes (distribution of participant nucleons in the transverse plane). The binary collision contribution is expected to be numerically small. Moreover the number of binary collisions is roughly $N_{part} - 1(2)$. The presence of a term depending on the number of binary collisions cannot be separated from the functional dependence on N_{part}. The number of participant nucleons in the Glauber model depends on the NN cross section.

p-Pb interactions at the LHC are planed at the c.m. energy in the NN system starting at $\sqrt{s_{NN}} = 4.4T$TeV. This corresponds to proton and Pb momenta of 3.5TeV and 208×1.38TeV, attainable with the present magnetic field configurations in the accelerator [7]. For deuteron beams it gives the energy $\sqrt{s_{NN}} = 3.11$TeV. The maximal available NN c.m. energy at the LHC is 8.8 and 6.22TeV for p-Pb and d-Pb interactions respectively. For collisions of beams with different energies per nucleon, the NN c.m. reference frame is shifted in rapidity with respect to the laboratory frame. The shift is $y_{sh} = 0.46$ and 0.12 for p-Pb and d-Pb interactions. All the calculations in the hydrodynamic model are made in the NN c.m. frame. For the final emitted particles a boost is made to the laboratory frame to get spectra around mid-rapidity or pseudorapidity distributions.

The NN cross section at different energies can be obtained from an interpolation of values at 200GeV 2.76TeV and 7TeV [25, 26] ($\sigma_{NN} = 42$, 62, and 71mb respectively) using a formula of the form $\sigma_{NN} \propto a + b\ln(\sqrt{s_{NN}}) + c\ln^2(\sqrt{s_{NN}})$. The resulting NN cross sections from the Table I are used in our Glauber model calculation. We take a Wood-Saxon profile for the Pb nuclear density

$$\rho(x,y,z) = \frac{\rho_0}{1 + \exp\left((\sqrt{x^2+y^2+z^2} - R_A)/a\right)}\ , \quad (2.1)$$

with $\rho_0 = 0.17\text{fm}^{-3}$, $R_A = 6.55$fm and $a = 0.45$fm, and an excluded distance for nucleons of 0.4fm, for the deuteron we use the Hulthen distribution [27].

Events at a given impact parameter are generated using the GLISSANDO code for the Glauber model [27].

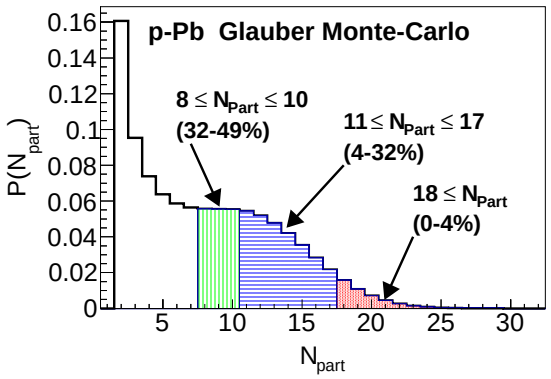

FIG. 2. (Color online) The probability distribution of participant nucleons in p-Pb interactions. The three centrality classes considered in the simulations are defined by cuts in the number of participant nucleons.

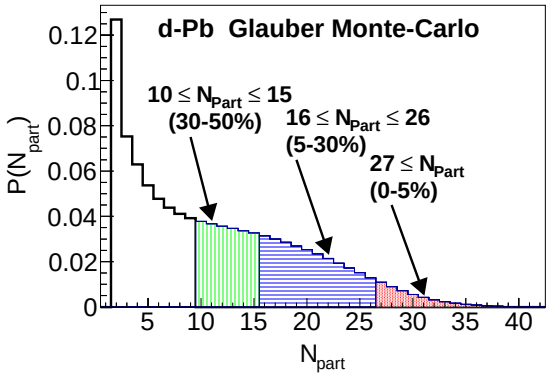

FIG. 3. (Color online) Same as Fig. 2 but for d-Pb interactions.

The distribution of participant nucleons at different impact parameters is shown in Fig. 1 for p-Pb interactions at 4.4TeV. We notice that the number of participant nucleons fluctuates strongly at a fixed impact parameter. The number of participant nucleons can be significantly above the average value (solid line in Fig. 1). Defining the most central collisions as a interval in the impact parameter is incorrect. The few percents most central events in terms of the number of participant nucleons ($N_{part} > 18$) have a participant multiplicity larger than the average N_{part} at zero impact parameter. The picture is very similar for d-Pb collisions. In the experiment the centrality classes are defined by the track multiplicity, closely correlated with the number of participants in the model. In heavy-ion collisions the number of participants is correlated with the impact parameter. In p-Pb or d-Pb interaction it is preferable to define the centrality classes for events using directly cuts in N_{part}. Figs. 2 and 3 show the probability density for events of a given N_{part} for the two systems considered. For p-Pb events, we use three centrality classes defined as $18 \leq N_{part}$, $11 \leq N_{part} \leq 17$, and $8 \leq N_{part} \leq 10$ corresponding to centrality bins $0-4\%$, $4-32\%$ and $32-49\%$ out of all the inelastic events ($N_{part} \geq 2$). The unusual numbers for the centrality percentiles are fixed by the discrete variable N_{part}. For the d-Pb interactions, we choose $27 \leq N_{part}$, $16 \leq N_{part} \leq 26$, and $10 \leq N_{part} \leq 15$ corresponding to centrality bins $0-5\%$, $5-30\%$ and $30-50\%$.

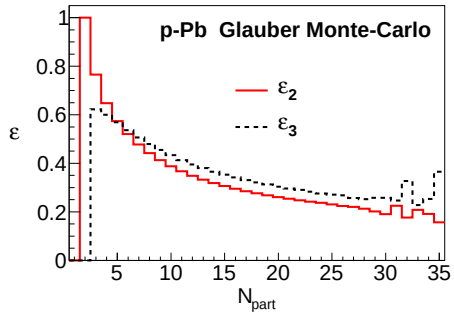

FIG. 4. (Color online) Eccentricity (solid line) and triangularity (dashed line) in p-Pb interactions as function of the number of participant nucleons.

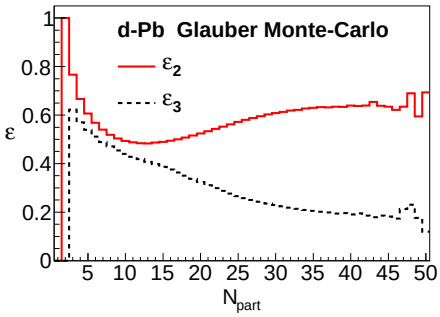

FIG. 5. (Color online) Same as Fig. 4 but for d-Pb interactions.

The charged particle density at central pseudorapidity can be estimated from the multiplicity observed at a similar energy and for a similar number of participant nucleons measured in peripheral Pb-Pb collisions at the LHC [9], interpolating the measured values of $dN/d\eta_{PS}$ / $< N_{part}/2 >$ at centralities $60-70\%$ and $70-80\%$ to the average number of participant nucleons $\langle N_{part} \rangle$ corresponding to the most central bins considered in p-Pb and d-Pb collisions. The energy dependence of dN/η_{PS} is $s^{0.11}$ for p-p and $s^{0.15}$ for nucleus-nucleus collisions [28]. We take $s^{0.13}$ to extrapolate from $\sqrt{s_{NN}} = 2.76$TeV. The estimated values of the charged particle density at midrapidity are quoted in Table I, the uncertainty comes from the uncertainty in the measurements [9] and in the value of the exponent in the energy dependence.

The azimuthally asymmetric collective flow is driven by the asymmetry of the initial fireball. The initial ec-

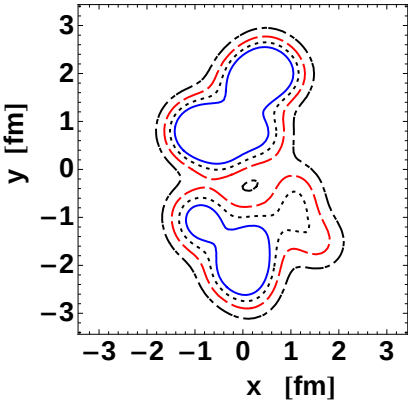

FIG. 6. (Color online) Contour plot $s(x, y, \eta_\parallel = 0)$ of the initial entropy density in a d-Pb collision with $N_{part} = 24$.

centricity in events with N_{part} participant nucleons

$$\epsilon_2 = \frac{\langle \sum_{i=1}^{N_{part}} r_i^2 \cos\left(2(\phi_i - \psi_2)\right)\rangle}{< \sum_{i=1}^{N_{part}} r_i^2 >} \tag{2.2}$$

is calculated in each event with respect to the eccentricity angle ψ_2 maximizing ϵ_2, the sum runs over all participant nucleons at positions r_i, ϕ_i, $\langle \dots \rangle$ denotes averaging over events. In a similar way the triangularity is

$$\epsilon_3 = \frac{\langle \sum_{i=1}^{N_{part}} r_i^3 \cos\left(3(\phi_i - \psi_3)\right)\rangle}{\langle \sum_{i=1}^{N_{part}} r_i^3 \rangle} \ , \tag{2.3}$$

and is calculated with respect the triangularity axis ψ_3 in each event [18, 19]. In Figs. 4 and 5 we plot the eccentricity and the triangularity as function of the number of participant nucleons in the fireball. In proton induced interactions, the eccentricity and the triangularity of the source are similar and decrease for central collisions. It is different for d-Pd collisions, the eccentricity is larger than the triangularity and increases for central events. The eccentricity in d-Pb interactions is caused by the asymmetric configuration of the two nucleons in the deuteron. Configurations with a large separation of the deuteron proton and neutron in the transverse plane have a large eccentricity and usually lead to a large number of participant nucleons in the Pb nucleus. This effect causes the increase of the eccentricity for the most central collisions in Fig. 5. We note that the eccentricity in Glauber models can be modified by correlation effects [27, 29]

We assume that the initial entropy density in the fireball is proportional to the number of participant nucleons. The density in the transverse plane x, y is the sum of contributions from participant nucleons at positions x_i, y_i from the Pb nucleus $N_-(x, y)$ and from the proton $N_+(x, y)$ (or from the proton and/or the neutron in the deuteron)

$$N_\pm(x, y) = s_0 \sum_i \frac{1}{2\pi\sigma_w^2} \exp\left(-\frac{(x - x_i)^2 + (y - y_i)^2}{2\sigma_w^2}\right) \ . \tag{2.4}$$

The contribution from each nucleon is a Gaussian of width $\sigma_w = 0.4$fm. The final results show some dependence on the chosen value of σ_w. Using a smaller width of 0.3fm/c we notice an increase by $\simeq 10\%$ of the integrated elliptic and triangular flow for p-Pb collisions. A similar effect has been observed in Ref. [22]. The parameter s_0 is fixed to reproduce the final multiplicity after the hydrodynamic evolution. The distribution in space-time rapidity $\eta_\parallel$ is asymmetric

$$s(x, y, \eta_\parallel) = f_-(\eta_\parallel) N_-(x, y) + f_+(\eta_\parallel) N_+(x, y) \ , \tag{2.5}$$

the profiles $f_\pm(\eta_\parallel)$ are of the form

$$f_\pm(\eta_\parallel) = \left(1 \pm \frac{\eta_\parallel}{y_{beam}}\right) f(\eta_\parallel) \ , \tag{2.6}$$

y_{beam} is the beam rapidity in the NN c.m. frame.

The asymmetric emission in the forward (backward) rapidity hemisphere from forward (backward) going nucleons can be observed in the distribution of charged particles in d-Au collisions at RHIC [30]. The distribution of the form (2.5) has been used as the initial condition for the hydrodynamic evolution in modeling Au-Au collisions at RHIC yielding a satisfactory description of the directed flow [31]. The parameters of the longitudinal profile

$$f(\eta_\parallel) = \exp\left(-\frac{(|\eta_\parallel| - \eta_0)^2}{2\sigma_\eta^2}\theta(|\eta_\parallel| - \eta_0)\right) \ , \tag{2.7}$$

the plateau width $2\eta_0$ and the width of the Gaussian tails σ_η are adjusted as initial conditions for $3 + 1$-D viscous hydrodynamic calculations to reproduce the charged particle pseudorapidity distributions in Au-Au collisions at 200GeV ($\eta_0 = 1.5$, $\sigma_\eta = 1.4$ [16]) and Pb-Pb collisions at 2.76TeV [28] ($\eta_0 = 2.3$, $\sigma_\eta = 1.4$). For the present calculation we take $\sigma_\eta = 1.4$ and $\eta_0 = 2.35$, 2.4 for interactions at 3.11 and 4.4TeV respectively. An example of the initial entropy density in a d-Pb interaction event in shown in Fig. 6. Typically we observe strongly deformed lumpy initial states. The elongated shape of the source results from the configuration of the nucleons in the deuteron while hitting the larger nucleus. This configuration is more important for the resulting eccentricity and the total number of participant nucleons than the impact parameter (as long as the deuteron hits the core of the Pb nucleus).

III. VISCOUS HYDRODYNAMICS

We use the second order relativistic viscous hydrodynamics to evolve the initial energy density in each event [32]. The initial entropy density is generated in the Glauber Monte-Carlo procedure described in the previous section. The viscous hydrodynamics incorporates deviations from local equilibrium in terms of the shear and bulk viscosities, at zero baryon density heat conductivity

can be neglected. These corrections $\pi^{\mu\nu}$ and Π to the energy momentum tensor $T^{\mu\nu}$ are evolved dynamically

$$\Delta^{\mu\alpha}\Delta^{\nu\beta}u^{\gamma}\partial_{\gamma}\pi_{\alpha\beta} = \frac{2\eta\sigma^{\mu\nu} - \pi^{\mu\nu}}{\tau_{\pi}} - \frac{4}{3}\pi^{\mu\nu}\partial_{\alpha}u^{\alpha} \quad (3.1)$$

and

$$u^{\gamma}\partial_{\gamma}\Pi = \frac{-\zeta\partial_{\gamma}u^{\gamma} - \Pi}{\tau_{\Pi}} - \frac{4}{3}\Pi\partial_{\alpha}u^{\alpha} \ . \quad (3.2)$$

$\Delta^{\mu\nu} = g^{\mu\nu} - u^{\mu}u^{\nu}$,

$$\sigma_{\mu\nu} = \frac{1}{2}\left(\nabla_{\mu}u_{\nu} + \nabla_{\mu}u_{\nu} - \frac{2}{3}\Delta_{\mu\nu}\partial_{\alpha}u^{\alpha}\right) \ , \quad (3.3)$$

and $\nabla^{\mu} = \Delta^{\mu\nu}\partial_{\nu}$. The hydrodynamic equations

$$\partial_{\mu}T^{\mu\nu} = 0 \quad (3.4)$$

are solved numerically in the proper time $\tau = \sqrt{t^2 - z^2}$ on a grid in the transverse coordinates x, y and the space-time rapidity $\eta_{\parallel}$, starting from $\tau_0 = 0.6$fm/c. We use $s_0 = 0.72\text{GeV}^3$ in (2.4) for both p-Pb and d-Pb collisions, which gives the expected final multiplicities. We take for the relaxation time $\tau_{\pi} = \frac{3\eta}{Ts}$, and assume $\tau_{\Pi} = \tau_{\pi}$. The initial fluid velocity u^{μ} is taken as the Bjorken flow, the initial stress corrections from shear viscosity correspond to the Navier-Stokes formula, while the initial bulk viscosity corrections are zero $\Pi(\tau_0) = 0$. The details of the solution in $2+1$-D and $3+1$-D are given in [12, 16].

The shear viscosity to entropy ratio in our calculation is not constant. It takes the value $\eta/s = 0.08$ in the plasma phase and increases in the hadronic phase [16]

$$\frac{\eta}{s}(T) = \frac{\eta_{HG}}{s}f_{HG}(T) + (1 - f_{HG}(T))\frac{\eta_{QGP}}{s} \quad (3.5)$$

with $\eta_{HG}/s = 0.5$, $\eta_{QGP}/s = 0.08$, and $f_{HG}(T) = 1/\left(\exp\left((T - T_{HG})/\Delta T\right) + 1\right)$, where $T_{HG} = 130$MeV, $\Delta T = 30$MeV. The bulk viscosity is nonzero in the hadronic phase

$$\frac{\zeta}{s}(T) = \frac{\zeta_{HG}}{s}f_{\zeta}(T) \quad (3.6)$$

with $\zeta_{HG}/s = 0.04$ and $f_{\zeta}(T) = 1/\left(\exp\left((T - T_{\zeta})/\Delta T_{\zeta}\right) + 1\right)$, where $T_{\zeta} = 160$MeV, $\Delta T_{\zeta} = 4$MeV. The equation of state is an interpolation of lattice QCD results at high temperatures [33] and a hadron gas model equation of state at lower temperatures. In constructing the equation of state we follow the procedure of [34]. The temperature dependence of the sound velocity has no soft point [16].

The hydrodynamic evolution stops at the freeze-out temperature of 135MeV. At the freeze-out hypersurface particle emission is done following the Cooper-Frye formula in the event generator THERMINATOR [35], with viscous corrections to the equilibrium momentum distribution f_0

$$f = f_0 + \delta f_{shear} + \delta f_{bulk} \quad (3.7)$$

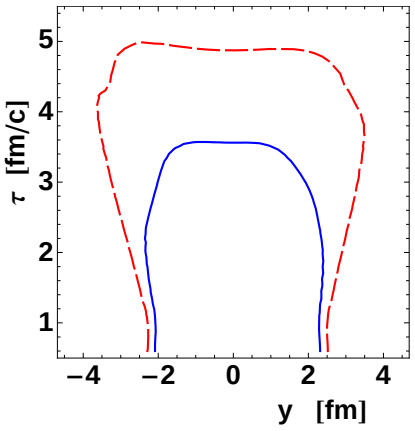

FIG. 7. (Color online) Constant temperature hypersurface $T(\tau, x = 0, y, \eta_{\parallel} = 0)$ in a p-Pb interaction for the freeze-out temperature $T_f = 135$MeV (dashed line) and for 160MeV (solid line).

We use quadratic corrections in momentum for the shear viscosity

$$\delta f_{shear} = f_0\left(1 \pm f_0\right)\frac{1}{2T^2(\epsilon + p)}p^{\mu}p^{\nu}\pi_{\mu\nu} \quad (3.8)$$

and asymptotically linear corrections for the bulk viscosity

$$\delta f_{bulk} = C_{bulk}f_0\left(1 \pm f_0\right)\left(c_s^2 u^{\mu}p_{\mu} - \frac{(u^{\mu}p_{\mu})^2 - m^2}{3u^{\mu}p_{\mu}}\right)\Pi \ , \quad (3.9)$$

with

$$\frac{1}{C_{bulk}} = \frac{1}{3}\sum_n \int \frac{d^3p}{(2\pi)^3}\frac{m^2}{E}f_0\left(1 \pm f_0\right)\left(c_s^2 E - \frac{p^2}{3E}\right) \ , \quad (3.10)$$

the sum runs over all the hadron species.

In Fig. 7 is shown the freeze-out hypersurface at $\eta_{\parallel} = 0$ for a p-Pb event with $N_{part} = 24$. The dense source survives for 5fm/c with the lifetime of the deconfined phase of 3.5fm/c ($T > 160$ MeV, solid line contour in Fig. 7).

IV. RESULTS

For each centrality class 50 hydrodynamic event are calculated. For each event several hundred THERMINATOR events are generated and analyzed together. This reduces non-flow effects, which in this case come from resonances decays. The numerical gird for the hydrodynamic evolution is set in the NN c.m. frame. The momenta of the emitted particles are boosted by $y_{sh} = 0.46$ and 0.12 for p-Pb and d-Pb collisions to obtain spectra in the LHC laboratory frame.

The distribution of charged particles in pseudorapidity is shown in Fig. 8 for the three centrality classes defined

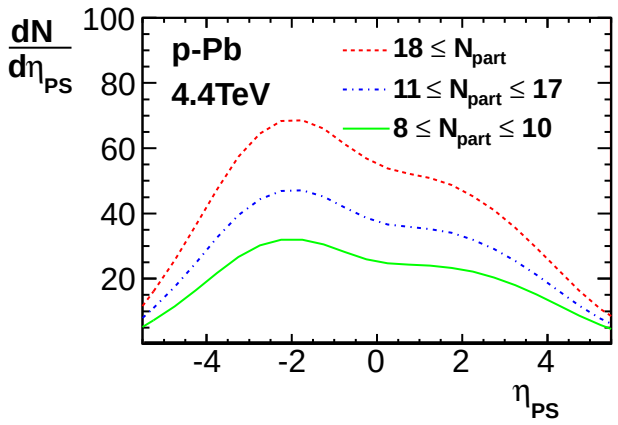

FIG. 8. (Color online) Pseudorapidity distribution of charged particles in p-Pb interactions at $\sqrt{s_{NN}} = 4.4$TeV. The dashed, dashed-dotted and solid lines correspond to the three centrality classes defined by the number of participant nucleons. The distributions are shown in the laboratory frame for the LHC experiments.

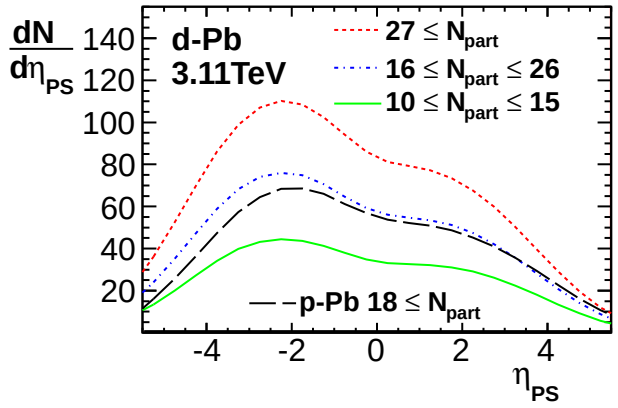

FIG. 9. (Color online) Same as Fig. 8 but for d-Pb interactions at $\sqrt{s_{NN}} = 3.11$TeV. The long-dashed line shows the pseudorapidity density for the most central p-Pb collisions at 4.4TeV.

in Sec. II. The density of charged particles at midrapidity for centrality bins $N_{part} \geq 18$ and $11 \leq N_{part} \leq 17$ in p-Pb is larger than observed in Pb-Pb collisions at 2.76TeV for centrality 70−80%. One can expect a similar degree of collective acceleration as in peripheral Pb-Pb events. The particle multiplicity in p-Pb interactions is of the same order as in p-p interactions with the highest multiplicity analyzed by the CMS collaboration [5]. While the nature of the high multiplicity p-p events is still unclear, the multiplicity in a p-Pb or d-Pb collision is simply related to the source size and density.

The charged particle densities in pseudorapidity for p-Pb (Fig. 8) and d-Pb collisions (Fig. 9) are asymmetric, reflecting the predominant emission from the participant

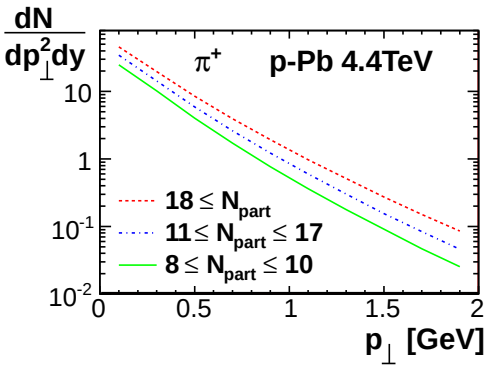

FIG. 10. (Color online) Transverse momentum spectra of π^+ in p-Pb interactions at $\sqrt{s_{NN}} = 4.4$TeV, for $y = 0$ in the laboratory frame. The dashed, dashed-dotted and solid lines correspond to the three centrality classes defined by the number of participant nucleons.

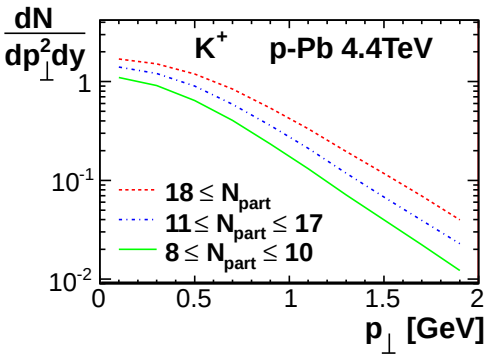

FIG. 11. (Color online) Same as Fig. 10 but for K^+.

nucleons in the Pb nucleus [30]. For d-Pb collisions in the centrality bin $N_{part} \geq 27$ the particle multiplicity is similar as in 60−70% centrality Pb-Pb interactions. This makes the applicability of the hydrodynamic model even more justified in that case. The particle multiplicity in

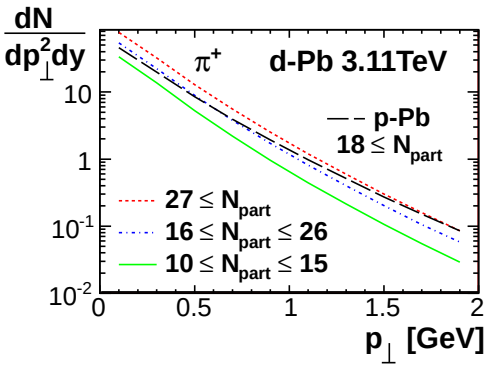

FIG. 12. (Color online) Same as Fig. 10 but for d-Pb interactions at $\sqrt{s_{NN}} = 3.11$TeV.

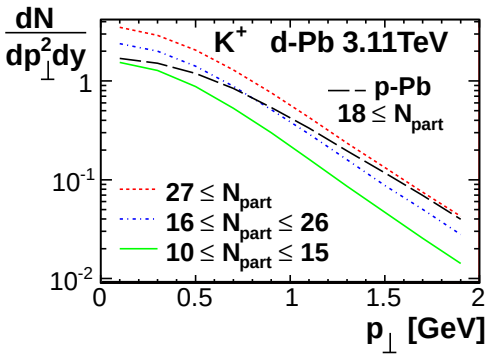

FIG. 13. (Color online) Same as Fig. 12 but for K^+.

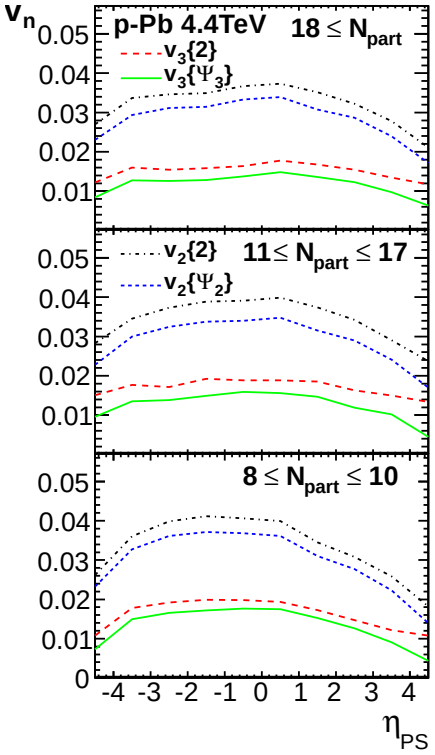

FIG. 14. (Color online) The elliptic and triangular flow coefficients of charged particles as function of pseudorapidity in the laboratory frame in p-Pb interactions, for centralities $0-4\%$ (top panel), $4-32\%$ (middle panel), and $32-49\%$ (bottom panel). The dashed-dotted and dotted lines represent the elliptic flow coefficients $v_2\{2\}$ and $v_2\{\Psi_2\}$, while the dashed and solid lines represent the triangular flow coefficients $v_3\{2\}$ and $v_3\{\Psi_3\}$.

p-Pb events with $N_{part} \geq 18$ is similar as for d-Pb events with $16 \leq N_{part} \leq 26$. We find, that in all the cases the charged particle density at midrapidity is to within 5% proportional to the number of participant nucleons.

The transverse momentum spectra for π^+ and K^+ emitted in p-Pb collisions are hardened by the collective transverse flow generated in the hydrodynamic expansion (Figs. 10 and 11). For more central collisions the spectra are slightly flatter, as more transverse flow is generated. A similar picture appears for transverse momentum spectra in d-Pb collisions. The spectra from $N_{part} \geq 27$ and $16 \leq N_{part} \leq 26$ centrality bins have a similar effective slope and are harder than the ones for the $10 \leq N_{part} \leq 15$ centrality class. It is interesting to observe that the transverse momentum spectra are harder in p-Pb than in d-Pb collisions. The transverse size of the fireball in p-Pb interactions is smaller but its density is higher, this leads to a faster transverse expansion than for d-Pb interactions.

Fluctuating initial densities (Fig. 6) have a nonzero eccentricity and triangularity (Fig. 4 and 5). The short hydrodynamical expansion stage in these systems is sufficient to generate noticeable elliptic and triangular flows. Fig. 14 shows the pseudorapidity dependence of the $p_\perp$ integrated elliptic v_2 and triangular v_3 flow coefficients in p-Pb interactions. In the calculations, 500 to 1500 THERMINATOR events are generated from each hypersurface generated in a 3+1-D viscous hydrodynamic evolution. The event plane orientations Ψ_2 and Ψ_3 are found and the elliptic v_2 and triangular v_3 flow coefficients are calculated in each event. The average over the hydrodynamic events gives $v_2\{\Psi_2\} = \langle v_2 \rangle$ and $v_3\{\Psi_3\} = \langle v_3 \rangle$. The second cumulant flow coefficients include flow fluctuations $v_n\{2\} = \sqrt{\langle v_n^2 \rangle}$. A moderate dependence of the elliptic and triangular flows on centrality is seen. In p-Pb collisions both the eccentricity and the triangularity deformations of the initial shape are fluctuation dominated. We observe some reduction of the collective flow at forward and backward pseudorapidities. This reduction is due to an increase of dissipative effects and a shorter life-time of the source at nonzero space-time rapidities [36, 37]. The form of the pseudorapidity dependence of the harmonic coefficients of the flow in Fig. 14 must be taken with caution, as 3+1-D viscous hydrodynamic calculations cannot reproduce it accurately [13, 16]. The azimuthally asymmetric flow is different in d-Pb collisions (Fig. 15). The elliptic flow is significantly larger than in p-Pb interactions, reaching 0.097 for central collisions. We notice a strong centrality dependence, v_2 increases significantly for central collisions. The initial eccentricity of the source in d-Pb collisions is large (Fig. 5). The elliptic flow fluctuations (the difference between $v_2\{2\}$ and $v_2\{\Psi_2\}$ [38]) are relatively less important for the deuteron than for the proton induced interactions. The triangular flow in d-Pb is similar as in p-Pb collisions, and does not vary strongly with the centrality.

The hydrodynamic response translates the initial deformation of the fireball into the azimuthal asymmetry of the final flow in an event by event basis. The elliptic flow coefficient follows closer the initial eccentricity than the triangular flow follows the initial triangularity, both in the magnitude and the orientation of the event plane. This observation is in agreement with other studies [39]. The hydrodynamic response v_2/ϵ_2 is larger for central collisions, where dissipative effects that reduce the flow

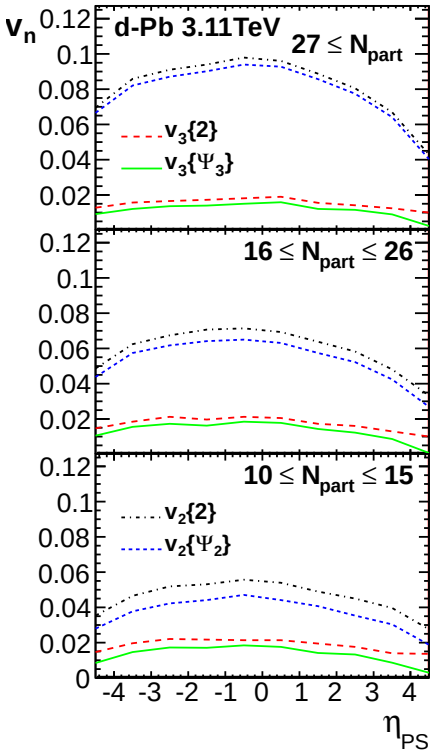

FIG. 15. (Color online) Same as Fig. 14 but for d-Pb interactions, for centralities $0-5\%$ (top panel), $5-30\%$ (middle panel), and $30-50\%$ (bottom panel).

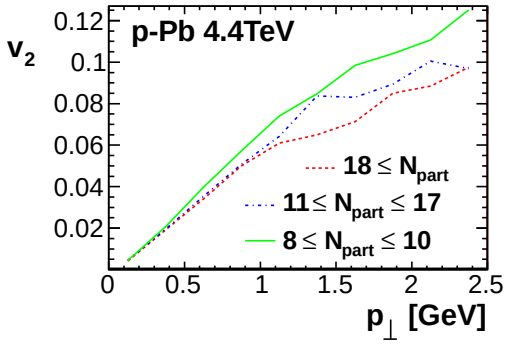

FIG. 16. (Color online) The elliptic flow coefficient of charged particles as function of transverse momentum around $y = 0$ in the laboratory frame for p-Pb interactions. The dashed, dashed-dotted and solid lines correspond to the three centrality classes defined by the number of participant nucleons, $N_{part} \geq 18$, $17 \geq N_{part} \geq 11$ and $10 \geq N_{part} \geq 8$ respectively.

asymmetry are smaller [40].

The elliptic and triangular flow coefficients show a hydrodynamic behavior as function of the transverse momentum (Figs. 16 and 18). Same as for the integrated flow, there is little change with centrality for the elliptic flow, while some decrease of v_3 in most central p-Pb collisions is seen. The elliptic flow $v_2(p_\perp)$ for the d-Pb

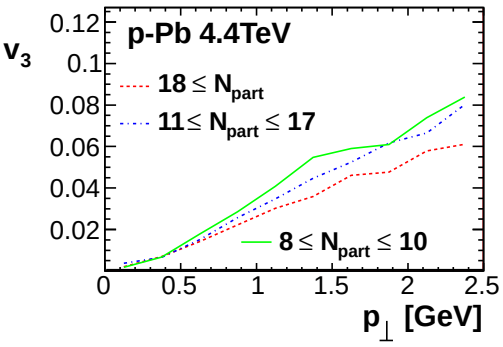

FIG. 17. (Color online) Same as Fig. 16 but for the triangular flow.

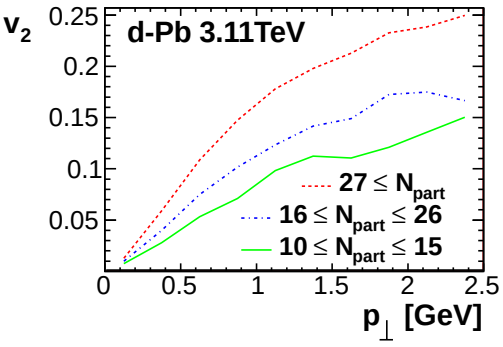

FIG. 18. (Color online) Same as Fig. 16 but d-Pb interactions. The dashed, dashed-dotted and solid lines correspond to the three centrality classes defined by the number of participant nucleons, $N_{part} \geq 27$, $26 \geq N_{part} \geq 16$ and $15 \geq N_{part} \geq 10$ respectively.

system (Fig. 18) is large, it increases significantly for central collisions, where a saturation of the dependence on the transverse momentum appears around 1GeV. The triangular flow in d-Pb interactions (Fig. 19) is similar in magnitude as in p-Pb collisions, and shows almost no

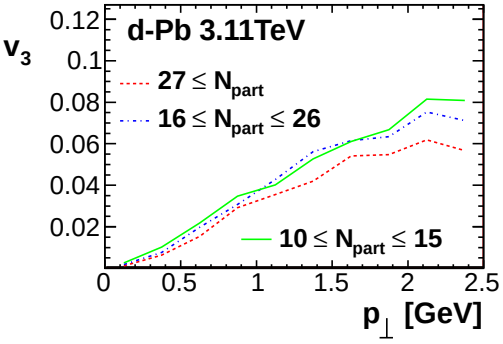

FIG. 19. (Color online) Same as Fig. 18 but for the triangular flow.

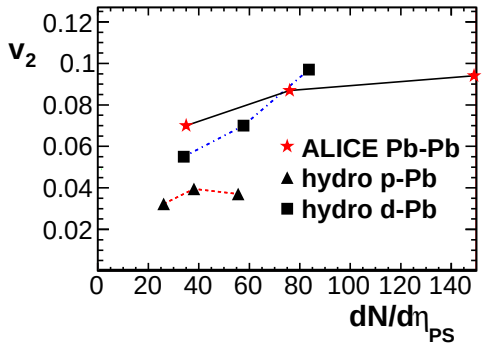

FIG. 20. (Color online) Elliptic flow coefficient $v_2\{2\}$ as function charge particle density at central pseudorapidity. Hydrodynamic calculations for p-Pb collisions at $\sqrt{s_{NN}} = 4.4$TeV (triangles), for d-Pb collisions at 3.11TeV (squares), and experimental data from the ALICE collaboration for Pb-Pb collisions at 2.76TeV (stars) [41] are shown.

variation with the centrality.

V. CONCLUSIONS

The formation of a hot, collectively expanding fireball in p-Pb collisions at $\sqrt{s_{NN}} = 4.4$TeV and d-Pb collisions at 3.11TeV is studied. We perform 3+1-D event by event viscous hydrodynamic calculations. The initial size and shape of the fireball is taken from the Glauber Monte-Carlo model. The initial entropy density is adjusted to reproduce the expected particle multiplicity estimated as an extrapolation from observations in peripheral Pb-Pb collisions at $\sqrt{s_{NN}} = 2.76$TeV.

A small hot and dense fireball is formed. It expands rapidly in the transverse direction. The $p_\perp$ spectra of emitted particles get harder, especially for p-Pb collisions. The deconfined phase survives for $3 - 4$fm/c in events with high particle multiplicity, the presence of such a dense medium should be visible in the nuclear attenuation factor for high $p_\perp$ hadrons. The size and the life-time of the source can be further constrained in same-pion interferometry measurements. The initial eccentricity and triangularity of a lumpy initial fireball lead to the formation of an azimuthally asymmetric flow. The elliptic flow is $3 - 4\%$ in p-Pb collisions, with little centrality dependence (Fig. 20). For the d-Pb system, the elliptic flow is significantly larger, increasing for central collisions, and reaching almost 10%. A comparison to peripheral Pb-Pb collisions in Fig. 20 shows that similar conditions are realized in proton or deuteron induced interactions. The elliptic flow of that magnitude can be measured, with a different dependence on centrality in p-Pb and d-Pb collisions.

Let us close with a discussion on future prospects for proton and deuteron induced reactions at ultrarelativistic energies. p-Pb collisions at 4.4TeV are planned in the near future at the LHC [7]. The elliptic flow and the hardening of the $p_\perp$ spectra are noticeable and should be looked for in the experimental analysis. However, it must be stressed that the dynamics of such small systems is at the limit of the applicability of the viscous hydrodynamic model. The use of the hydrodynamic model in d-Pb interactions is better justified, also the elliptic flow is stronger, but such collisions are not planned in the near future at the LHC. The shift to the maximum LHC energy to $\sqrt{s_{NN}} = 6.22$ for d-Pb and 8.8TeV for p-Pb collisions results in an increase of the particle multiplicity by 30%. Hydrodynamic expansion would last longer, with less dissipative effects. The eccentricity and triangularity are similar as at lower LHC energies and qualitatively we expect similar results.

In view of the results in this paper it seems very interesting to look for collective effects in d-Au collisions at $\sqrt{s_N} = 200$GeV in RHIC experiments. The multiplicity in central d-Au interactions is similar as in peripheral Au-Au collisions at the same energy. If some stage of collective expansion is present, the large initial eccentricity in a d-Au system should translate into a measurable elliptic flow. Unfortunately no published data exist for these experiments, hydrodynamical simulations are underway.

ACKNOWLEDGMENTS

Supported by Polish Ministry of Science and Higher Education under grant N N202 263438. Numerical calculations were made on the Cracow Cloud One cluster.

[1] I. Arsene *et al.* (BRAHMS), Nucl. Phys. **A757**, 1 (2005)B. B. Back *et al.* (PHOBOS), *ibid.* **A757**, 28 (2005)J. Adams *et al.* (STAR), *ibid.* **A757**, 102 (2005)K. Adcox *et al.* (PHENIX), *ibid.* **A757**, 184 (2005)
[2] K. Aamodt *et al.* (ALICE), Phys.Rev.Lett. **105**, 252302 (2010)Phys. Lett. **B696**, 328 (2011)G. Aad *et al.* (Atlas), Phys. Rev. Lett. **105**, 252303 (2010)S. Chatrchyan *et al.* (CMS), Phys. Rev. **C84**, 024906 (2011)
[3] M. Luzum and P. Romatschke, Phys. Rev. Lett. **103**, 262302 (2009)
[4] D. d'Enterria *et al.*, Eur. Phys. J. **C66**, 173 (2010)P. Bożek, Acta Phys. Pol. **B41**, 837 (2010)J. Casalderrey-Solana and U. A. Wiedemann, Phys. Rev. Lett. **104**, 102301 (2010)E. Avsar, C. Flensburg, Y. Hatta, J.-Y. Ollitrault, and T. Ueda(2010), arXiv:1009.5643 [hep-ph]
[5] V. Khachatryan *et al.* (CMS), JHEP **09**, 091 (2010)
[6] K. Aamodt *et al.* (ALICE)(2011), arXiv:1101.3665 [hep-ex]P. Bożek, Eur.Phys.J. **C71**, 1530 (2011)K. Werner, I. Karpenko, and T. Pierog,

Phys.Rev.Lett. **106**, 122004 (2011)
[7] C. Salgado, J. Alvarez-Muniz, F. Arleo, N. Armesto, M. Botje, *et al.*(2011), arXiv:1105.3919 [hep-ph]
[8] A. Dumitru, D. E. Kharzeev, E. M. Levin, and Y. Nara(2011), arXiv:1111.3031 [hep-ph]G. Barnafoldi, J. Barrette, M. Gyulassy, P. Levai, and V. Topor Pop(2011), arXiv:1111.3646 [nucl-th]D. Kharzeev, E. Levin, and M. Nardi, Nucl.Phys. **A747**, 609 (2005)P. Quiroga-Arias, J. G. Milhano, and U. A. Wiedemann, Phys.Rev. **C82**, 034903 (2010)A. H. Rezaeian and A. Schafer, **D81**, 114032 (2010)C. A. Salgado, J.Phys.G **G38**, 124036 (2011)
[9] K. Aamodt *et al.* (ALICE), Phys. Rev. Lett. **106**, 032301 (2011)
[10] P. F. Kolb and U. W. Heinz, in *Quark Gluon Plasma 3*, edited by R. Hwa and X. N. Wang (World Scientific, Singapore, 2004) arXiv:nucl-th/0305084P. Huovinen and P. V. Ruuskanen, Ann. Rev. Nucl. Part. Sci. **56**, 163 (2006)W. Florkowski, *Phenomenology of Ultra-Relativistic Heavy-Ion Collisions* (World Scientific Publishing Company, Singapore, 2010)
[11] M. Luzum and P. Romatschke, Phys. Rev. **C78**, 034915 (2008)A. K. Chaudhuri, Phys. Rev. **C74**, 044904 (2006)P. Huovinen and D. Molnar, Phys. Rev. **C79**, 014906 (2009)H. Song and U. W. Heinz, Phys. Lett. **B658**, 279 (2008)K. Dusling and D. Teaney, Phys. Rev. **C77**, 034905 (2008)
[12] P. Bożek, Phys. Rev. **C81**, 034909 (2010)
[13] B. Schenke, S. Jeon, and C. Gale, Phys. Rev. Lett. **106**, 042301 (2011)
[14] D. Teaney, J. Lauret, and E. V. Shuryak, Phys. Rev. Lett. **86**, 4783 (2001)P. Huovinen, in *Quark Gluon Plasma 3*, edited by R. Hwa and X. N. Wang (World Scientific, Singapore, 2004) arXiv:nucl-th/0305064W. Broniowski, M. Chojnacki, W. Florkowski, and A. Kisiel, Phys. Rev. Lett. **101**, 022301 (2008)S. V. Akkelin, Y. Hama, I. A. Karpenko, and Y. M. Sinyukov, Phys. Rev. **C78**, 034906 (2008)
[15] T. Hirano and K. Tsuda, Phys. Rev. **C66**, 054905 (2002)Y. Hama *et al.*, Nucl. Phys. **A774**, 169 (2006)C. Nonaka, J. Phys. **G34**, S313 (2007)P. Bożek and I. Wyskiel, Phys. Rev. **C79**, 044916 (2009)
[16] P. Bożek(2011), arXiv:1110.6742 [nucl-th]
[17] R. Andrade, F. Grassi, Y. Hama, T. Kodama, and J. Socolowski, O., Phys. Rev. Lett. **97**, 202302 (2006)K. Werner *et al.*, J. Phys. **G36**, 064030 (2009)H. Petersen, G.-Y. Qin, S. A. Bass, and B. Muller, Phys.Rev. **C82**, 041901 (2010)
[18] B. Alver *et al.*, Phys. Rev. **C77**, 014906 (2008)
[19] B. Alver and G. Roland, Phys. Rev. **C81**, 054905 (2010)
[20] B. H. Alver, C. Gombeaud, M. Luzum, and J.-Y. Ollitrault, Phys. Rev. **C82**, 034913 (2010)
[21] Z. Qiu and U. W. Heinz(2011), arXiv:1108.1714 [nucl-th]
[22] B. Schenke, S. Jeon, and C. Gale(2011), arXiv:1109.6289 [hep-ph]B. Schenke, S. Jeon, and C. Gale, Phys.Lett. **B702**, 59 (2011)
[23] P. Bożek, Phys. Lett. **B699**, 283 (2011)
[24] C. Shen, U. Heinz, P. Huovinen, and H. Song, Phys.Rev. **C84**, 044903 (2011)
[25] C. Loizides (ALICE), J.Phys.G **G38**, 124040 (2011)
[26] G. Aad *et al.* (ATLAS), Nat. Commun. **2**, 463 (2011)
[27] W. Broniowski, M. Rybczyński, and P. Bożek, Comput. Phys. Commun. **180**, 69 (2009)
[28] A. T. Toia (ALICE), J.Phys.G **G38**, 124007 (2011)
[29] W. Broniowski and M. Rybczynski, Phys.Rev. **C81**, 064909 (2010)M. Rybczynski and W. Broniowski(2011), arXiv:1110.2609 [nucl-th]
[30] A. Białas and W. Czyż, Acta Phys. Polon. **B36**, 905 (2005)
[31] P. Bożek and I. Wyskiel, Phys. Rev. **C81**, 054902 (2010)
[32] W. Israel and J. Stewart, Annals Phys. **118**, 341 (1979)
[33] S. Borsanyi *et al.*, JHEP **11**, 077 (2010)
[34] M. Chojnacki and W. Florkowski, Acta Phys. Polon. **B38**, 3249 (2007)
[35] M. Chojnacki, A. Kisiel, W. Florkowski, and W. Broniowski(2011), arXiv:1102.0273 [nucl-th]
[36] T. Hirano, U. W. Heinz, D. Kharzeev, R. Lacey, and Y. Nara, Phys. Lett. **B636**, 299 (2006)
[37] P. Bożek and I. Wyskiel, PoS **EPS-HEP 2009**, 039 (2009)
[38] S. A. Voloshin, A. M. Poskanzer, A. Tang, and G. Wang, Phys. Lett. **B659**, 537 (2008)
[39] F. G. Gardim, F. Grassi, M. Luzum, and J.-Y. Ollitrault(2011), arXiv:1111.6538 [nucl-th]A. Chaudhuri(2011), arXiv:1112.1166 [nucl-th]
[40] H.-J. Drescher, A. Dumitru, C. Gombeaud, and J.-Y. Ollitrault, Phys. Rev. **C76**, 024905 (2007)
[41] K. Aamodt *et al.* (ALICE), Phys.Rev.Lett. **107**, 032301 (2011)